Time Resolved PIV Analysis of a Gurney flap on a NACA 0015 Airfoil

D. R. Troolin, E.K. Longmire, W. T. Lai

Abstract A NACA 0015 airfoil with and without a Gurney flap was studied in a wind tunnel where $Re_c = 2.1 \times 10^5$ in order to examine the evolving flow structure of the wake through time-resolved PIV and to correlate this structure with time-averaged measurements of the sectional lift coefficient. The Gurney flap is a tab of small length (1% to 4% of the airfoil chord) that protrudes 90° to the chord at the trailing edge. The Gurney flap increases the lift on an airfoil while increasing the drag only minimally for cases where the height of the flap is within the boundary layer region. Multiple vortex shedding modes were seen upstream and downstream of the Gurney flap.

1 Introduction

Aerodynamic design has seen a rise in the implementation of multifunctional devices and actuators that allow for dramatic changes in performance with only slight variations to the effective surfaces. Although rote airfoil design has essentially yielded its peak in performance, auxiliary mechanisms are being investigated and explored for their potential in making airfoils more functional, especially in demanding environments such as edge-of-the envelope performance, unmanned light and fast, and high-lift low-speed applications.

The Gurney flap, a small tab approximately 1% to 4% of the airfoil chord in length that protrudes typically 90° to the chord at the trailing edge, is one such device (Figure 1).

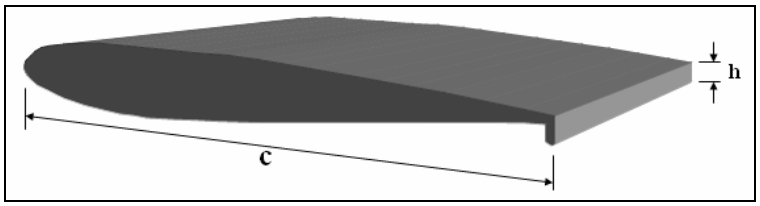

Figure 1: Gurney flap on an airfoil.

Originally used on a racecar in the 1970's by Daniel Gurney, for whom it is named, the flap was first studied at some length by Liebeck (1978). Subsequent studies include water investigations by Neuhart and Pendergraft (1988), which gave information on the flow structure. Wadcock performed two-dimensional wind tunnel tests at a Reynolds Number of 1.64×10^6 on a baseline NACA 4412 at the NASA Ames 7 by 10 foot Wind Tunnel (1987). These tests showed a significant increase in the lift coefficient, shifting the lift curve up by 0.3 for a Gurney flap of 1.25% of the chord length, and providing a higher maximum lift. There was no appreciable increase in drag until the Gurney flap was extended beyond about 2% of the airfoil chord length. Storms et al. studied the Gurney flap in connection with vortex generators (1994). Maughmer et al. investigated the Gurney flap for miniature trailing edge effectors for rotorcraft applications (2003). A numerical method was employed by Jang et al. (1998), LDA measurements by Jeffrey et al.(2000), and time-averaged PIV (Particle Image Velocimetry) analysis by Solovitz and Eaton (2004) to gather additional information on the flow pattern around Gurney flaps. Practically speaking, the flap has seen applications from banner-towing aircraft (see Wynbrandt 2002), to unmanned air vehicles (UAV's) as investigated by Solovitz and Eaton (2004).

This study quantifies the effects of a Gurney flap on a NACA 0015 airfoil through time-averaged force measurements, hot film anemometry, and time-resolved particle image velocimetry (TRPIV). A high-speed laser and a high frame-rate camera were used to capture the formation and subsequent shedding of vortices downstream of airfoils with smooth and flapped trailing edges. The phenomena such as time-resolved vortical interactions as well as shedding frequency were explored to add insight into the overall flow characteristics.

D. R. Troolin, W. T. Lai, TSI Incorporated, 500 Cardigan Road, Shoreview, MN 55126, USA
E. K. Longmire, Department of Aerospace Engineering and Mechanics, University of Minnesota, Minneapolis, MN 55455, USA

Correspondence to:
D. R. Troolin, TSI Incorporated, 500 Cardigan Rd., Shoreview, MN 55126, E-mail: dan.troolin@tsi.com

2
Experimental Apparatus

The experiments were conducted using the University of Minnesota Aerospace Engineering Return Open Wind Tunnel. The test section is 0.6 m × 0.6 m square. Hot-film anemometry measurements show a freestream turbulence intensity of less than 0.25%. The airfoil section had a wing span (b) of 304.8 mm and a chord length (c) of 190.5 mm, resulting in an aspect ratio of $A = 0.49$. The airfoils and flap attachments were made in a rapid-prototype machine at the University of Minnesota Department of Aerospace Engineering and Mechanics. The airfoil was mounted to a flat, circular, aluminum plate and was then mounted to the wind tunnel sting (Figure 2).

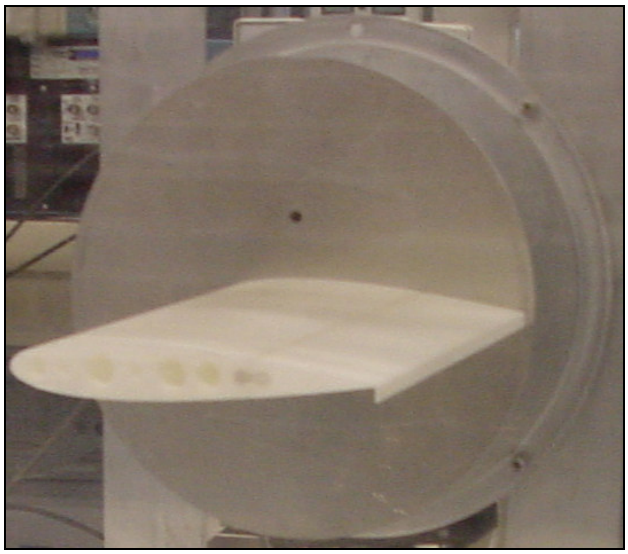

Figure 2: Airfoil section mounted in wind tunnel.

There were four Gurney flap configurations, with the length of the Gurney flap (h) measured relative to the total chord length of the airfoil: 0%, 1%, 2%, and 4%. This study concentrates on the airfoil with the 4% Gurney flap. The control configuration consisted of a NACA 0015 symmetric airfoil without a Gurney flap. This design was chosen, as it is a very common airfoil (there is a large body of experimental data available) and the NACA 0015 has a fairly simple design. The control airfoil was tested for purposes of repeatability and comparison.

In the wind tunnel, the airfoil was secured against a flat plate on one side, and for the force measurements, placed very close (~2 mm) to the wall of the wind tunnel on the other side. This set-up gave somewhat the effect of an infinite aspect ratio. The TRPIV tests were performed at approximately the middle of the wind tunnel and middle of the airfoil section. Since the 3-D effects of the wingtip interactions are minimized, the airfoil testing more closely resembles a 2-D airfoil. When compared with values published by NACA (National Advisory Committee on Aeronautics) on the same airfoil section, and corrected for infinite aspect ratio, the characteristics of the control airfoil matched very well with lift coefficient (see Jacobs et al. 1937).

The force measurements, hot-film anemometry, and TRPIV data were conducted at a freestream velocity of U_∞ = 15.89 m/s. The Reynolds number based on chord length was $Re_c = 2.1 \times 10^5$. The TRPIV measurements were made in two configurations. The first was with the laser light sheet entering from the exit of the tunnel, and the second had the light sheet entering the tunnel from above. The camera was on the side of the tunnel as seen in Figure 3. The data from the second configuration has been inverted in the subsequent plots for purposes of comparison.

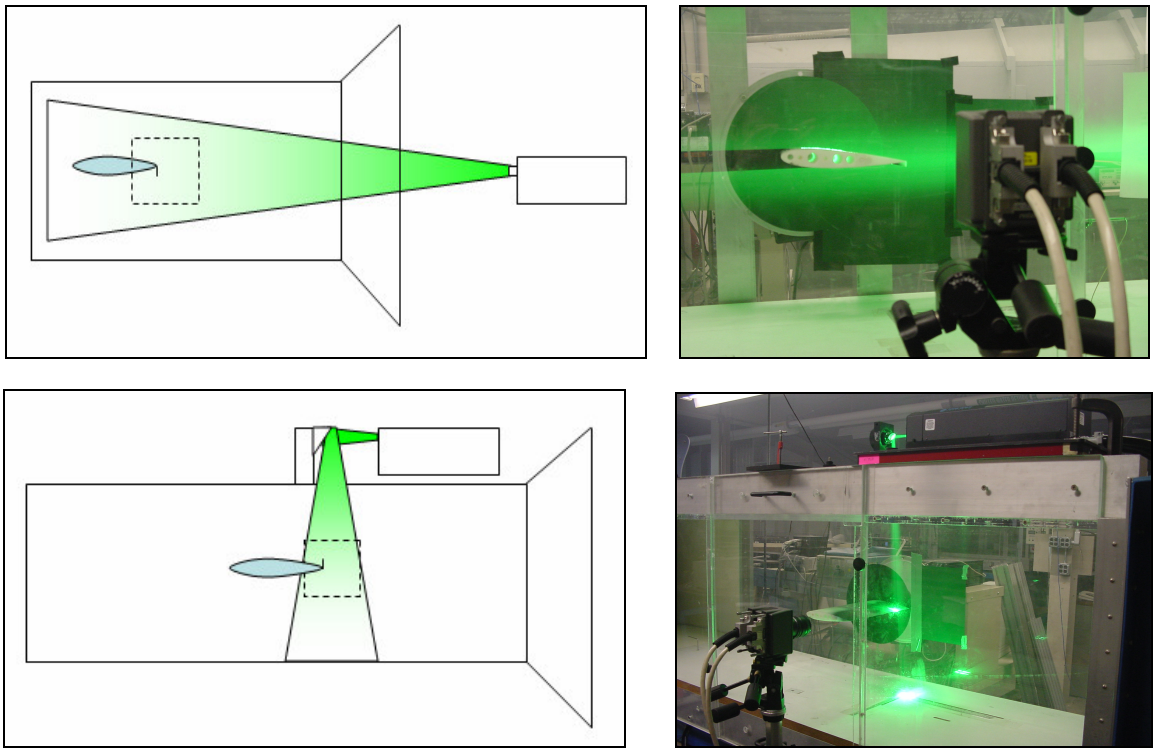

Figure 3: Schematic of the experimental setup in the wind tunnel. Upper two figures show configuration one; lower two figures show configuration two.

These two configurations allowed velocity information to be gleaned from the area directly downstream of the Gurney flap, as well as from the cavity directly upstream of the flap. The laser was a 30 W diode pumped Nd:YLF system, emitting light of wavelength 527 nm. The light sheet thickness was approximately 2 mm. At 2000 frames per second, the energy per pulse was 10 mJ, and at 8000 the energy per pulse was 4 mJ.

The digital image sequences were acquired from a 10-bit CMOS high speed camera at rates of 2000 frames per second, 4000 frames per second, and 8000 frames per second, which correspond to velocity field capture rates of 1000 Hz, 2000 Hz, and 4000 Hz, respectively. In this paper, we concentrate primarily on the data captured at 2000 frames per second with full camera pixel resolution of 1024 by 1024 pixels, and on data captured at 8000 frames per second with pixel resolution of 1024 by 256 pixels. The pixel size is 9 microns. The distance from the camera to the light sheet varied from 400 mm to 550 mm. A 50 mm lens was used with a largest aperture setting of f#1.4. The full field of view was 114 mm square. The Δt value was 35 μs, which allowed for a maximum particle displacement of 4 pixels at U_∞ = 15.89 m/s. Olive oil atomized with an array of six Laskin nozzles was used to seed the flow, providing droplets with a mean diameter between 1 μm and 3 μm.

For each run, between 50 and 500 TRPIV velocity fields were acquired. The vector fields were determined using a CDIC deformation algorithm described by Wereley and Gui (2001). This four-pass method used an interrogation region of 16 by 16 pixels with 75% overlap, which corresponds to a resolution of slightly more than 2 mm. The first two passes consisted of a recursive grid to determine integer pixel displacement values. The following two passes employed the four-corner deformation grid. This processing scheme provided 97% or higher valid vectors.

2 Results

Force Measurements

Force measurements were taken on the airfoil at a Reynolds number of $Re_c = 2.1 \times 10^5$. The results of the sectional lift coefficient ($C_L = L'/½\rho U_\infty^2 c$) vs. angle of incidence (α) are presented in Figure 4 for various flap heights (h); the uncertainty in lift coefficient was ±0.065. The shape of the lift curve versus angle of incidence remains nearly identical for airfoils with Gurney flaps as compared to the control airfoil without a Gurney flap; however, the maximum C_L is raised from 1.05 for the airfoil without a Gurney flap, to 1.21 for a 1% Gurney flap, then to 1.40 for

a 2% Gurney flap, and finally to 1.60 for a 4% Gurney flap. A possible argument for the increase in lift caused by the flaps is that the velocity over the pressure surface of the airfoil must be reduced by the presence of the Gurney flap, therefore increasing the circulation. A proof of this argument would require detailed velocity measurements around the entire airfoil, however.

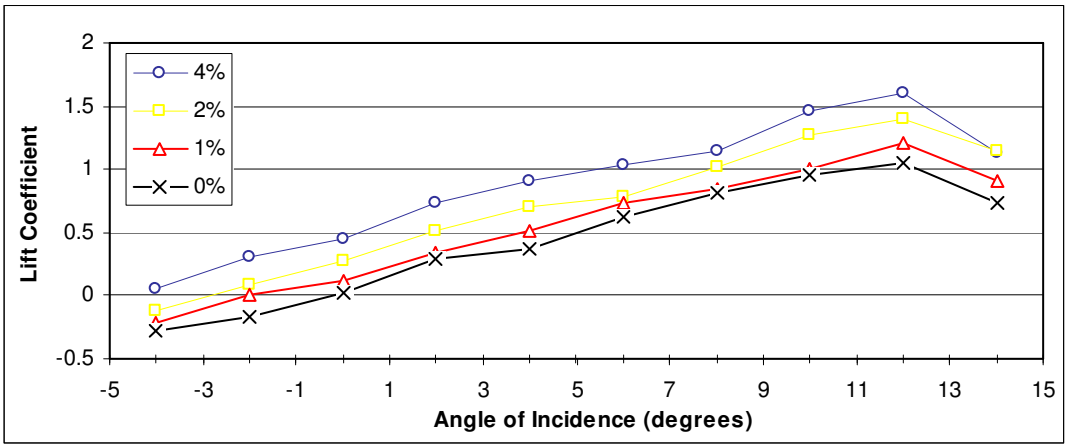

Figure 4: C_L vs. α for Gurney flaps of various heights.

A point of interest is that, for the cases examined, the increase in maximum lift coefficient is not linear with increasing flap height. The increase in maximum lift coefficient seen for the 1% flap is 15%, while the increases for the 2% and 4% flaps are 33% and 52%, respectively. As the size of the flap is increased, the benefit it provides in increased lift begins to diminish. This trend and the overall curve shapes are consistent with the findings of Wadcock (1987) and Jeffrey et al. (2000).

Hot-film Anemometry Measurements

A hot film was placed at a distance of 0.5c directly downstream of the trailing edge for the airfoil without a Gurney flap, and directly downstream of the lowest point of the flap for the 4% Gurney airfoil. Power spectra were obtained from samples of 8,000 points collected at a sampling rate of 2,000 Hz. Spectra were also determined independently using TRPIV velocity field data, to determine the validity of this method for calculating spectra. In this case, the FFT was based on the average fluctuating velocity normal to the freestream direction (v') within a region (nine vectors square) approximately 0.5c directly downstream of the trailing edge, or directly downstream of the lowest point of the 4% Gurney flap. The sampling rate was 1,000 Hz; the number of samples was 300.

The airfoil without the Gurney flap displayed a typical frequency spectrum (not shown) without any dominant peak. The spectra for the airfoil with the 4% Gurney flap had an obvious peak whose frequency value showed a strong dependence upon the angle of incidence. Peak frequencies obtained with both methods are shown in Figure 5 in the form of Strouhal number vs. angle of incidence. The plot demonstrates that TRPIV frequency analysis matches well with the hot film anemometry, and is a valid technique for obtaining the frequency of fluctuating velocity in this case.

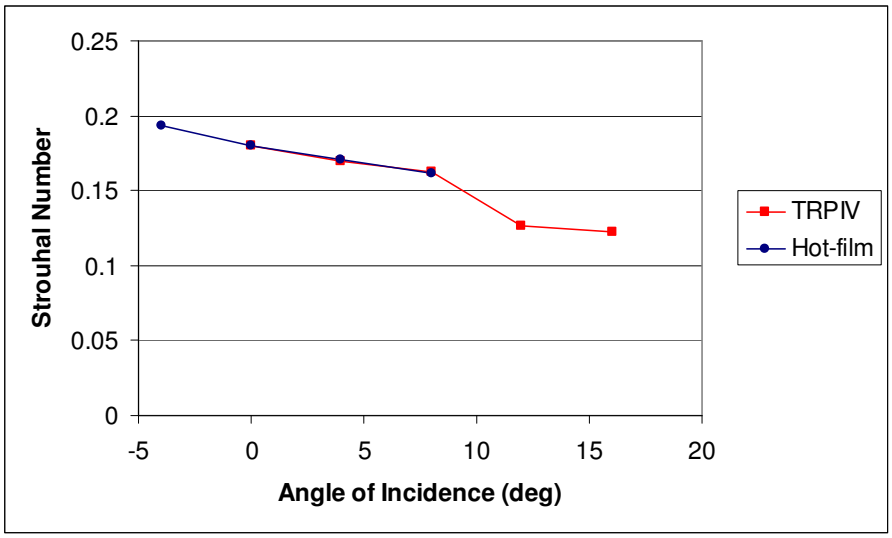

Figure 5: Strouhal number ($St = fh/U_\infty$) vs. α for 4% Gurney flap.

The frequency analysis suggests the presence of alternating positive and negative vortices being shed downstream of the Gurney flap. The Strouhal number for the vortex shedding was determined by analyzing the frequency (f) peaks as they related to the Gurney height (h) and the freestream velocity (U_∞). A strong relationship was witnessed between the angle of incidence of the airfoil (α) and the resulting Strouhal number ($St = fh/U_\infty$), as can be seen in Figure 5 in which the Strouhal numbers are plotted vs. the various α as calculated by hot-film anemometry and TRPIV. As α is increased from α = -4° to α = 8°, the Strouhal number decreases linearly from 0.19 to 0.16. Frequency spectra plotted for other airfoil shapes have resulted in similar trends and magnitudes for the Strouhal number (see Jeffrey et al. 2000).

Ensemble-Averaged PIV Measurements

The time-averaged velocity magnitude field with streamlines can be seen in Figure 7 for a 4% Gurney flap at α = 0°, 4°, 8°, and 12°. Fifty consecutive fields, corresponding with approximately 18 cycles of vortex shedding, were averaged, and the results are normalized by the freestream velocity U_∞.

The plots show that the area of decreased velocity directly downstream of the Gurney flap increases in length as the angle of incidence increases. At α = 0°, the zone of strongly reduced velocity (depicted as blue) is compact, and the higher speed flows on either side of the airfoil recover fairly quickly after the separation behind the flap. This recovery takes longer as α is increased until α = 12° which is the approximate stall angle. Note also that the wake (or zone of reduced velocity) is turned downward as α increases. The streamlines are also turned downward with increasing α as expected from the lift measurements. The 'average' separated region depicted by the streamlines shows a relatively symmetric vortex pair at α = 0° that becomes increasingly asymmetric as α is increased. At α = 12°, a negative vortex dominates the area directly downstream of the Gurney, while a more compact, positive vortex has been shifted downstream. These results agree well with the time-averaged velocity fields determined by Jeffrey, et al. (2000) and others (see Jang et al. 1998 and Solovitz and Eaton 2004).

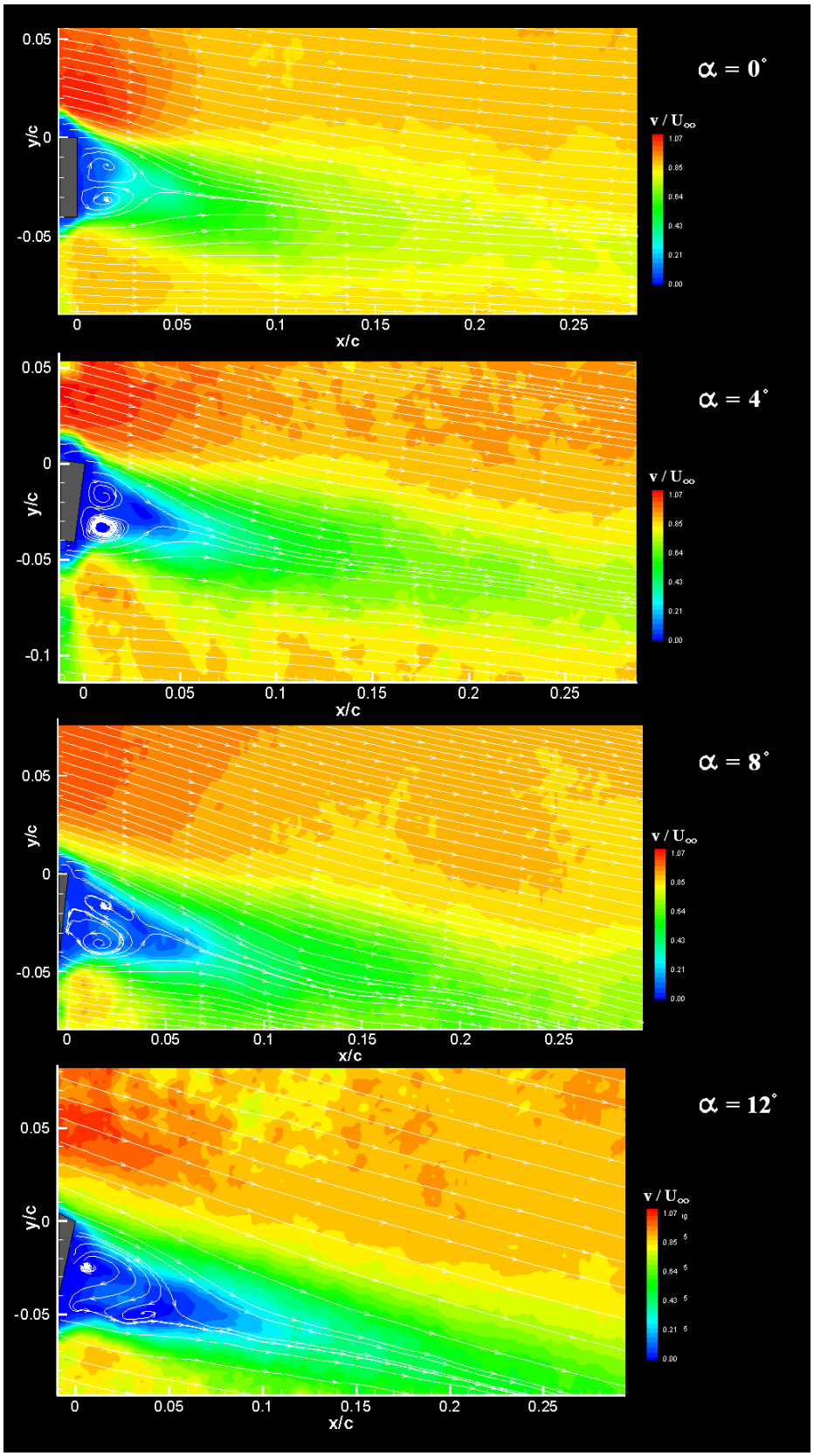

Figure 6: Time-averaged velocity magnitude for 4% Gurney flap with α = 0°, 4°, 8° and 12°, respectively.

Time-Resolved PIV Measurements

Vortex shedding and subsequent interactions occur at the boundary of two separating shear layers, and the resulting interaction forms the well-known Kármán vortex street (see Kuethe and Chow 1998). The Gurney flap acts as a bluff body which produces vortex shedding, but its asymmetry yields asymmetries in the wake pattern. Of particular interest in this study was the path of the vortices as they formed and were convected downstream.

The TRPIV flow sequences for $\alpha = 0°$ and $\alpha = 8°$ (see Figures 7 and 8) reveal that strips of spanwise vorticity (ζ) with negative and positive sign are shed from the upper airfoil surface and Gurney flap tip respectively. In Figure 7 ($\alpha = 0°$), the vorticity shed from the upper surface remains focused in the form of a strip that is pulled downward into the flap wake. The positive vorticity shed from the flap tip is spread initially over a larger length scale across the wake, and shows greater intermittency in the streamwise direction. Downstream of the trailing edge, the wake develops into an asymmetric Kármán vortex street pattern. The areas of negative vorticity appear more focused than the areas of positive vorticity. The wake also exhibits a net downward flow direction which is expected given the positive lift coefficient for this configuration. The wake asymmetry can be explained partially by the differences in flow direction at the airfoil trailing edge and the flap tip. The presence of the flap generates a local separation upstream so that the streamlines are diverted downward compared with the 'no flap' configuration. Separate plots of normalized streamwise velocity (u/U_∞) show significant variations in magnitude immediately below the flap tip indicating intermittent shedding of fluid from the separated zone upstream of the flap. In Figure 8 ($\alpha = 8°$), the vorticity from the upper surface is again pulled into the flap wake in the form of strips. The ensuing wake is then characterized by increased disorder and asymmetry compared to the $\alpha = 0°$ case. Regions of positive and negative vorticity can be distinguished, but there is less focusing of the structures, which manifest themselves in many smaller patches rather than neat bundles. Further downstream of the flap, the small patches of positive and negative vorticity are tightly intertwined suggesting greater disorganization in the wake. The normalized streamwise velocity plot emphasizes the increased disorder seen in the vorticity plot, and the region beneath the flap tip shows increased fluctuations in magnitude from the $\alpha = 0°$ case.

The Gurney flap sequences can be contrasted with a 'no flap' sequence in Figure 9. As would be expected, this velocity sequence reveals a much narrower wake with much weaker velocity deficits. In addition, any coherent vortical structures are weaker and less defined. When the angle of incidence is increased to 8°, the wake remains narrow but is deflected downward as expected.

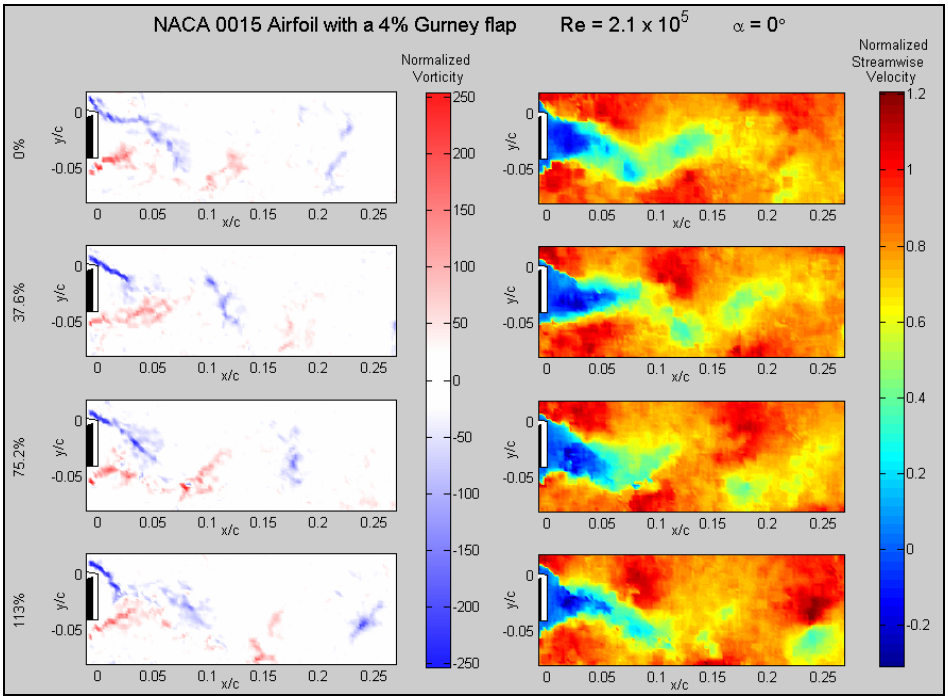

Figure 7: Normalized vorticity ($\zeta c/U_\infty$) (left), and normalized streamwise velocity (u/U_∞) (right) downstream of the 4% Gurney flap on a NACA 0015 airfoil at $\alpha = 0°$. Phase values on the right indicate the percentage of one complete shedding cycle. The capture rate was 1000 Hz (2000 fps).

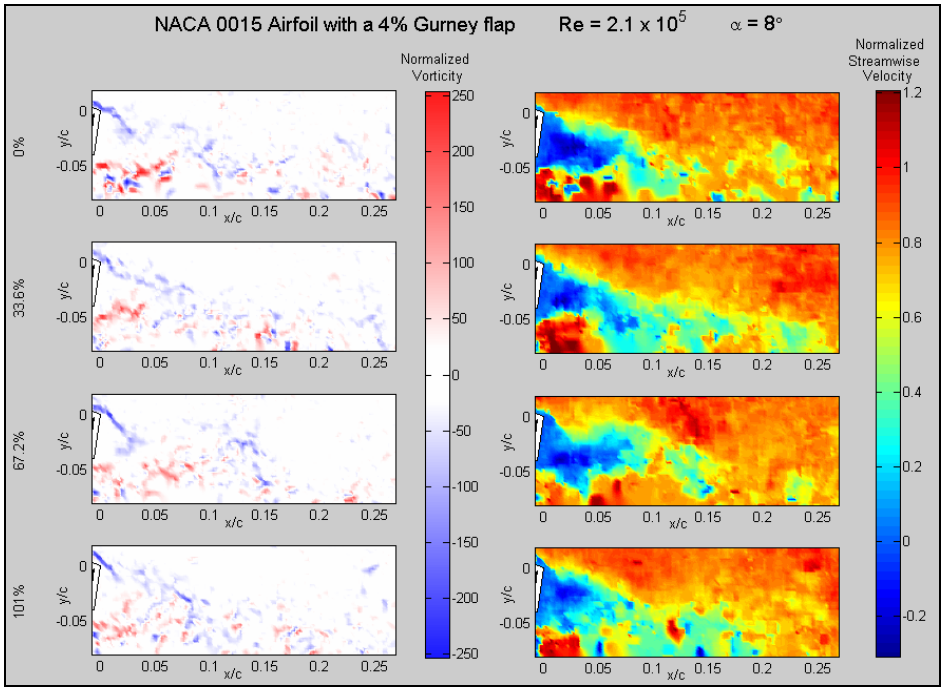

Figure 8: Normalized vorticity ($\zeta c/U_\infty$) (left), and normalized streamwise velocity (u/U_∞) (right) downstream of the 4% Gurney flap on a NACA 0015 airfoil at α = 8°. Phase values on the right indicate the percentage of one complete shedding cycle. The capture rate was 1000 Hz (2000 fps).

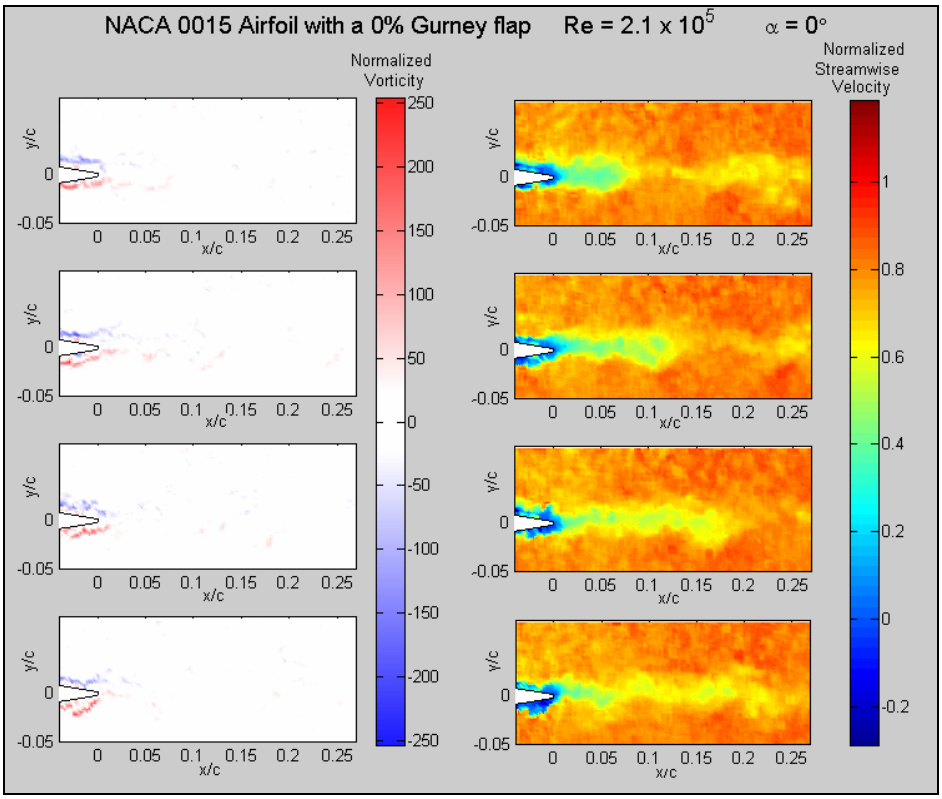

Figure 9: TRPIV sequence captured at 1000 Hz (2000 fps) for the control airfoil without the Gurney flap at α = 0°. Column on the left shows normalized vorticity, while the column on the right shows normalized streamwise velocity.

TRPIV data taken with the laser sheet directed through the top of the wind tunnel allowed the cavity upstream of the Gurney flap to be examined. In this case, the flapped airfoils were inverted compared with those in the previous studies. For ease of comparison with the previous results, the plots in this section have been inverted to match the previous geometries.

Figures 10 and 11 exhibit the 2D swirl strength and the normal velocity around the tip of the Gurney flap for $\alpha = 0°$ and $\alpha = 8°$. Two-dimensional swirl is a quantity used to identify vortices with significant strength, and cores normal to the measurement plane. If the discriminant of the characteristic equation of the two-dimensional velocity gradient tensor is less than zero, then the 2D swirl strength is defined as the imaginary part of its complex root (see Adrian et al. 2000). The swirl is normalized by the freestream velocity and the chord length. Also, the swirl (a positive scalar quantity) is given a sign indicating the direction of the corresponding vorticity. The phase values shown to the left of each plot were calculated based on the Strouhal number determined in the hot film anemometry and TRPIV frequency measurements. The swirl strength plots show distinct alternating positive and negative vortex cores being generated asymmetrically downstream of the flap, with a negative streamwise and negative normal velocity trajectory.

For the $\alpha = 0°$ case (Figure 10), the 0% phase plot reveals a positive vortex core forming on the downstream edge of the Gurney flap tip. The core then moves downstream and slightly downward in the subsequent phases. Approximately half way through the cycle, a negative vortex core is seen separating from the upper surface, and continuing downstream and slightly downward in the airfoil wake. The normal velocity plot (right column) gives emphasis to the large spatial velocity gradients.

Figure 11 plots the $\alpha = 8°$ case. The same general structure can be seen in terms of the vortex shedding; however, consistent with the previous vorticity plots (Figure 8), the ensuing wake is less organized as evidenced by the less coherent vortex cores.

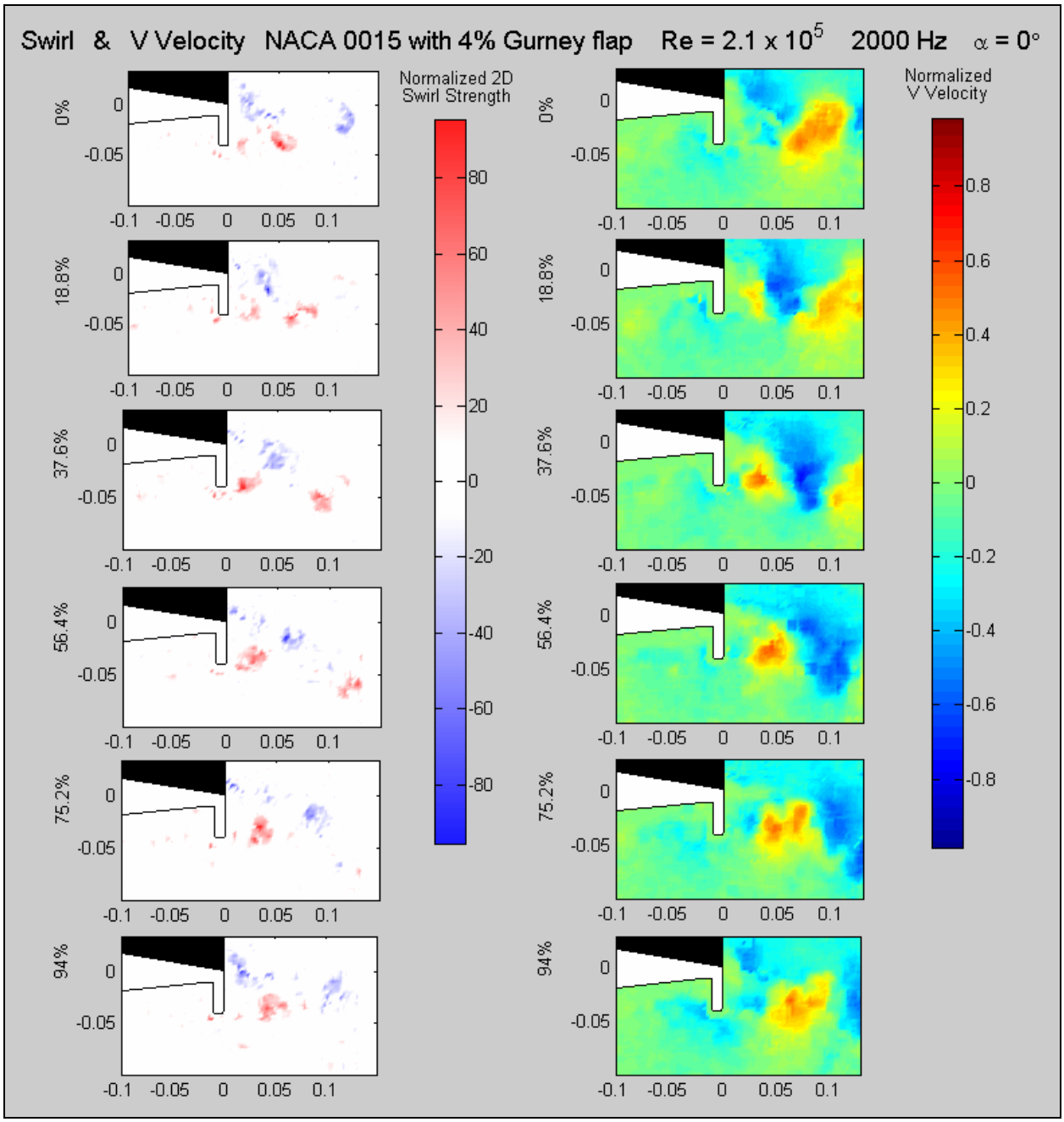

Figure 10: One full primary vortex shedding sequence for the case of a 4% Gurney flap at α = 0° captured at 4000 Hz (8000 fps), every other frame is shown. The phase values to the left of each plot represent the percentage of one complete vortex shedding sequence. The plots display the normalized 2D swirl strength (left) and the normalized normal velocity (right).

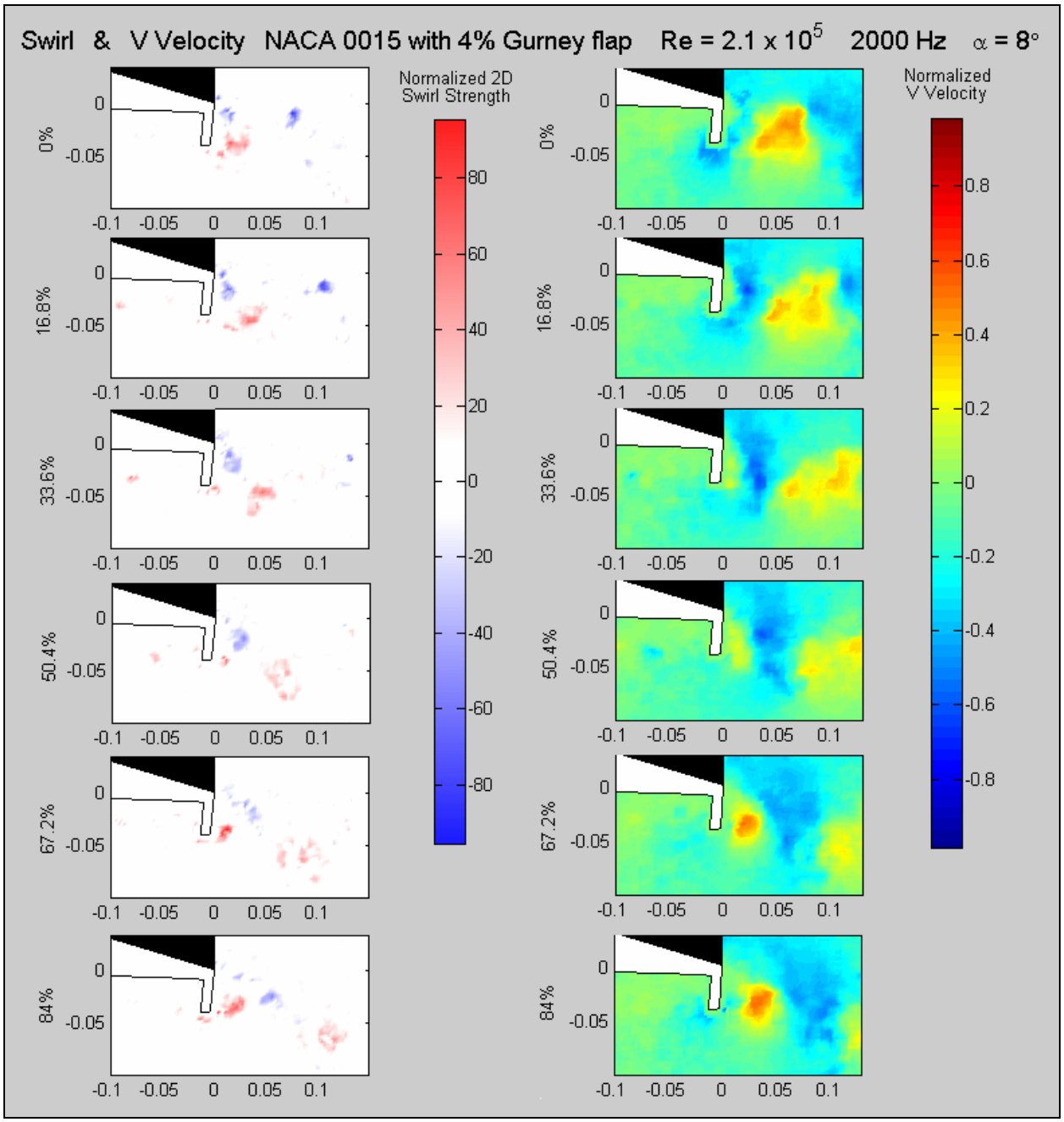

Figure 11: One full primary vortex shedding sequence for the case of a 4% Gurney flap at α = 8° captured at 4000 Hz (8000 fps), every other frame is shown. The phase values to the left of each plot represent the percentage of one complete vortex shedding sequence. The plots display the normalized 2D swirl strength (left) and the normalized normal velocity (right).

The asymmetric vortex shedding downstream of the Gurney flap is immediately apparent in the swirl strength and normal velocity sequence plots (Figures 10 and 11), which were captured at 4000 Hz (every other frame is shown). The asymmetry is due to several modes of vortex shedding occurring off of the flap tip. Careful studies of time-resolved movies created with sequences of streamwise and normal velocity revealed the nature of the different vortex shedding modes, as seen in Figure 12, where the slower moving fluid in the upstream cavity agglomerates (phases 0% and 18.8%), grows (phase 37.6%), and is expunged into the wake (phase 56.4%).

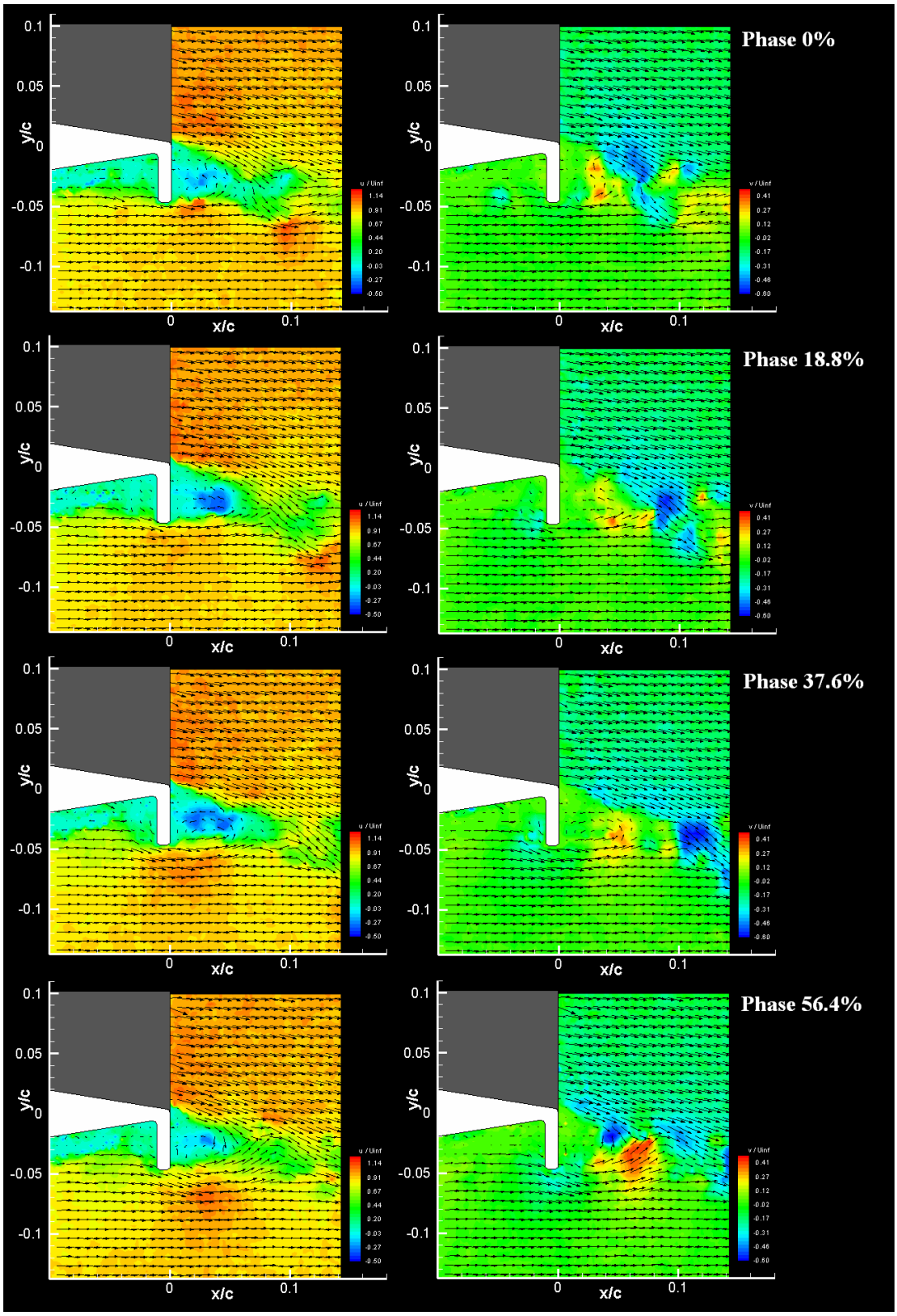

Figure 12: Four consecutive instantaneous velocity fields of the airfoil with 4% Gurney flap taken at 2000 Hz corresponding to phase positions of 0%, 18.8%, 37.6%, and 56.4%, showing the interaction of the upstream portion of the flap with the oncoming streamwise velocity in the form of instantaneous velocity vectors overlaid on normalized streamwise velocity (u/U_∞) (left) and normalized normal velocity (v/U_∞) (right).

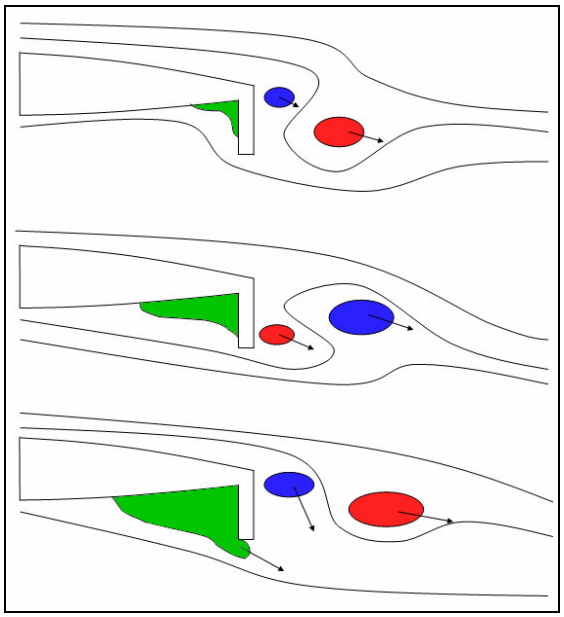

Figure 13: Schematic of the bimodal vortex shedding occurring at the trailing edge of the airfoil with a Gurney flap. Positive vorticity is indicated in red; negative vorticity is indicated in blue. The green areas represent fluid "trapped" in the upstream cavity. Arrows represent general trajectories of certain flow structures.

Figure 13 displays a schematic of the two types of vortex shedding seen in the data and in the previous figure. PIV sequences and wake visualization show that the flap creates a forward facing step which traps fluid in the form of a weak and generally disorganized positive vortex (shown in green). The fluid cannot escape above through the airfoil, or downstream due to the flap. Neither can the slow moving fluid escape downward as this would require it to cross the fast-moving, nearly streamwise velocity present below the airfoil but outside of the boundary layer. While slow-moving boundary layer fluid from beneath the airfoil is accumulating in the cavity upstream of the Gurney flap, the airfoil and flap support a shape resembling an asymmetric solid body with a blunt trailing edge. Streamlines nominally attach to this shape before shedding off of the trailing edge with a frequency of 375 Hz (St = 0.18) for the case of $\alpha = 0°$. After some amount of time, the fluid that has been accumulating in the upstream cavity has grown spatially, both downward toward the flap tip and also upstream in the direction of the leading edge, to the point where its length scale is near that of the Gurney flap height. When this occurs, the trapped vortex achieves enough energy to penetrate the layer of high streamwise velocity just below the Gurney flap. This is manifested in a burst of velocity downward, as the vortex escapes the cavity, and an accompanying burst in streamwise velocity. This downward velocity component induces a similar downward component of velocity on the fluid and vortex structures directly downstream of the Gurney flap. During this instant, the flow behind the flap achieves a relatively large component of negative normal velocity that momentarily increases the circulation on the airfoil, thus increasing the lift. This also helps to explain the shape and deflection of the time-averaged velocity magnitude plots in Figure 6. A histogram of the normal velocity measured at the tip of the Gurney flap can be seen in Figure 14; its bimodal distribution indicates normal velocity in primarily two modes, when the upstream vortex is weak but gaining strength, and when the vortex is expunged from the cavity.

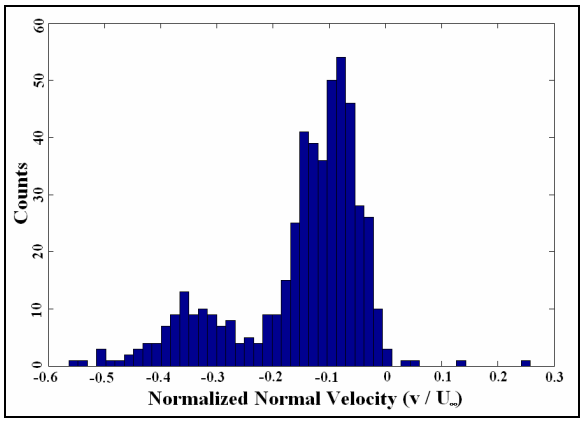

Figure 14: Normalized normal velocity histogram at the point adjacent to the Gurney flap tip.

Observations and frequency analysis upstream of the Gurney flap using the TRPIV data, indicate that the frequency at which the trapped fluid is expunged from the upstream cavity is somewhat lower than that of the Kármán shedding frequency, though the frequency peaks are weaker than those downstream of the flap. For the case of the airfoil at $\alpha = 0°$ with the 4% Gurney flap, the dominant frequency in the region of the cavity was 250 Hz ($St = 0.12$). The airfoil without the Gurney flap was also studied; the examination yielded no evidence of strong swirl strength or normal velocity for the $\alpha = 0°$ case.

3 Conclusions

The Gurney flap is a device that increases the lift on an airfoil while inducing only a limited amount of drag, adding an overall gain to the airfoil design. While it is somewhat intuitive that the Gurney flap increases lift by adding to the effective camber of the wing, the less-obvious advantage of the Gurney flap lies in the intriguing interaction of the counter-rotating vortices that are alternately shed downstream, as well as the vortices being shed from the cavity upstream of the Gurney flap tip. The symmetric airfoil comes to a point at the trailing edge and leaves a weak and narrow wake. The Gurney design requires the turbulent flow downstream of the airfoil to follow a fairly structured set of paths which are the alternating counter-rotating vortices. Further, boundary layer fluid in the cavity upstream of the Gurney flap is trapped and intermittently released into the wake which in turn induces a net negative normal velocity on the airfoil wake increasing the circulation, and thus the lift. While the Gurney flap did not increase the stall angle of incidence, the flow it induced did serve to increase the lift at every angle of incidence measured.

Acknowledgements

Special thanks to the University of Minnesota Aerospace Engineering and Mechanics Department for the use of the facilities and fabrication of the airfoil test sections.

5 References

Adrian R; Christensen K; Liu Z; (2000) Analysis and interpretation of instantaneous turbulent velocity fields. Exp. Fluids 29, pp. 275-290.

Jacobs; Eastman; N Sherman; Albert (1937) Airfoil section characteristics as affected by variations of the Reynolds number, NACA Langley Memorial Aeronautical Laboratory (Langley Field, VA, United States) NACA Report 586, 41 pp.

Jang C; Ross J; Cummings R (1998) Numerical investigation of an airfoil with a Gurney flap. Aircraft Design 1, pp. 75-88.

Jeffrey D; Zhang X; Hurst D (2000) Aerodynamics of Gurney Flaps on a Single-Element High-Lift Wing, Journal of Aircraft, Vol. 37. No. 2, pp. 295-301.

Kuethe A; Chow C (1998) Foundations of Aerodynamics: Bases of Aerodynamic Design 5th Ed. New York: John Wiley & Sons, Inc.

Liebeck R (1978) Design of subsonic airfoils for high lift. Journal of Aircraft 15(9), pp. 547-61.

Maughmer M; Lesieutre G; Koopmann G (2003) Miniature Trailing Edge Effectors for Rotorcraft Applications. Natl. Rotorcraft Tech. Center.

Neuhart D; Pendergraft O (1988) A water tunnel study of Gurney flaps. NASA TM 4071.
Solovitz S; Eaton J (2004) Spanwise Response Variation for Partial-Span Gurney-Type Flaps, AIAA Journal, Vol 42, No. 8, pp. 1640-1643.
Solovitz S; Eaton J (2004) Dynamic Flow Response Due to Motion of Partial-Span Gurney-Type Flaps, AIAA Journal, Vol 42, No. 9, pp. 1729-1736.
Storms B; Jang C (1994) Lift Enhancement of an Airfoil Using a Gurney Flap and Vortex Generators, J. Aircraft, Vol. 31, No. 3, pp. 542-547.
Wadcock A (1987) Investigations of low-speed turbulent separated flow around airfoils. NASA CR 177450.
Wereley S; Gui L (2001) PIV measurement in a four-roll-mill flow with a central difference image correction (CDIC) method, 4th International Symposium on Particle Image Velocimetry, Göttingen, Germany, September 17.
Wynbrandt J (2002) Ban, or Banner? AOPA Pilot, pp. 97-101.